A sensitivity analysis of q-space indices with respect to changes in axonal diameter, dispersion and tissue composition

Rutger Fick, Marco Pizzolato, Demian Wassermann, Mauro Zucchelli, Gloria Menegaz, Rachid Deriche

A SENSITIVITY ANALYSIS OF Q-SPACE INDICES WITH RESPECT TO CHANGES IN AXONAL DIAMETER, DISPERSION AND TISSUE COMPOSITION

R.H.J. Fick[⋆] *M. Pizzolato*[⋆†] *D. Wassermann*[⋆] *M. Zucchelli*[‡] *G. Menegaz*[‡] *R. Deriche*[⋆]

[⋆] Athena Project-Team, Inria Sophia Antipolis - Méditerranée, France
[‡] Department of Computer Science, University of Verona, Verona, Italy

ABSTRACT

In Diffusion MRI, q-space indices are scalar quantities that describe properties of the ensemble average propagator (EAP). Their values are often linked to the axonal diameter – assuming that the diffusion signal originates from inside an ensemble of parallel cylinders. However, histological studies show that these assumptions are incorrect, and axonal tissue is often dispersed with various tissue compositions. Direct interpretation of these q-space indices in terms of tissue change is therefore impossible, and we must treat them as scalars that only give non-specific contrast – just as DTI indices. In this work, we analyze the sensitivity of q-space indices to tissue structure changes by simulating axonal tissue with changing axonal diameter, dispersion and tissue compositions. Using human connectome project data, we then predict which indices are most sensitive to tissue changes in the brain. We show that, in both multi-shell and single-shell (DTI) data, q-space indices have higher sensitivity to tissue changes than DTI indices in large parts of the brain. Based on these results, it may be interesting to revisit older DTI studies using q-space indices as markers for pathology.

Index Terms— Diffusion MRI, MAP-MRI, q-space Indices, NODDI, Axonal Dispersion, Axonal Diameter

1. INTRODUCTION

An important application in diffusion MRI (dMRI) is to infer pathology-related tissue changes from properties of the ensemble average propagator (EAP) [1]. Recently, functional basis approaches have allowed for the estimation of so-called q-space indices that describe various properties of the three-dimensional EAP [2, 3]. In contrast to Diffusion Tensor (DT) indices [4], q-space indices also describe the restricted, i.e., *non-Gaussian* aspects of the EAP. Because of this, q-space indices allow us to relate the EAP to microstructural properties such as the axon diameter, but only when we assume that the tissue consists of parallel cylinders with no extra-axonal space [5]. However, from histological studies, we know that both these assumptions are incorrect and even in the Corpus Callosum we must account for axonal dispersion [6]. This means that q-space indices cannot directly be linked to tissue microstructure, and must be treated as values that only provide non-specific tissue contrast, just as DT indices.

In this work, we analyze the sensitivity of q-space indices to microstructural changes in the presence of axonal dispersion. Inspired by [7], we measure the sensitivity of a q-space index as its partial derivative with respect to changes in axonal diameter, dispersion, and volume fractions of intra-axonal and isotropic signal contributions (Figs. 1 and 2). We also compare with the sensitivity of classical DT-indices to the same microstructure changes. Finally, we show on high-quality data of the Human Connectome Project (HCP) [8] which index would be most sensitive to a particular change in microstructure (Fig. 3).

2. MATERIALS AND METHODS

In this section, we explain our processing pipeline from data generation to q-space index sensitivity analysis. We first provide our dMRI acquisition scheme and our simulation model. We then briefly explain our method of estimating q-space indices. Lastly, we explain the sensitivity analysis.

Acquisition Parameters: We use the multi-shell acquisition scheme of the MGH-HCP database [8] in our experiments. This data has particularly high b-values $\{0,\ 1000,\ 3000,\ 5000,\ 10000\}$ s/mm^2 with $\{40, 64, 64, 128, 256\}$ directions and $1.5\,\text{mm}^3$ isotropic voxels. The pulse length and separation time are $\delta/\Delta = 12.9/21.8\,\text{ms}$. Assuming rectangular pulses the q-space positions are defined as $\mathbf{q} = (\gamma\delta\mathbf{G})/2\pi$. When comparing with DT-indices, we fit DTI tensors to a single-shell $b_{\text{max}} = 1000\,\text{s/mm}^2$ acquisition by cutting the outer three shells of the multi-shell acquisition.

Signal Generation: We generate diffusion data corresponding to dispersed cylinders using the orientation-dispersed white matter model [9]

$$E = (1 - \nu_{iso})(\nu_{ic}E_{ic} + (1 - \nu_{ic}) * E_{ec}) + \nu_{iso}E_{iso} \quad (1)$$

with $E_{ic}(a, ODI)$ the intra-axonal signal with cylinder diameter a and Orientation Dispersion Index (ODI). The signal inside the cylinders is given by the Gaussian Phase Approximation and the dispersion is given by the Watson model,

[†]The author expresses his thanks to Olea Medical and to the Provence-Alpes-Côte d'Azur Regional Council for providing grant and support.

where ODI goes from 0 (no dispersion) to 1 (completely dispersed). The free water signal E_{iso} is an isotropic tensor with free water diffusivity $3{\cdot}10^{-9}m^2/s$ and the extra-axonal signal $E_{ec}(\kappa)$ is a *dispersed* anisotropic tensor with perpendicular diffusivity $1.2 \cdot 10^{-9}m^2/s$, with ν_{ic} and ν_{iso} the intra-axonal and isotropic volume fractions.

Signal Fitting and EAP Reconstruction: We use the Laplacian-regularized Mean Apparent Propagator (MAP)-MRI basis [3, 5] to reconstruct the EAP. In short, MAP-MRI fits the signal with a set of orthogonal basis functions as $E(\mathbf{q}) = \sum_i^{N_{\max}} \mathbf{c}_i \Phi_{N_i}(\mathbf{q})$ where every basis function Φ_{N_i} is given as a product of three 1D functions

$$\Phi_{N_i}(\mathbf{A}, \mathbf{q}) = \phi_{n_{x(i)}}(u_x, q_x)\phi_{n_{y(i)}}(u_y, q_y)\phi_{n_{z(i)}}(u_z, q_z) \quad (2)$$
$$\text{with} \begin{cases} \phi_n(u,q) = \frac{i^{-n}}{\sqrt{2^n n!}} e^{-2\pi^2 q^2 u^2} H_n(2\pi u q) \\ \mathbf{A} = \text{Diag}(u_x^2, u_y^2, u_z^2) \end{cases}$$

with basis order $N_i = (n_{x(i)}, n_{y(i)}, n_{z(i)})$. We find the diagonalized scaling factors $\mathbf{A} = \mathbf{R}\mathbf{A}'\mathbf{R}^T$ by fitting a tensor $\mathbf{A}'$, where $\mathbf{R}$ contains the tensor eigenvectors. We then rotate the data into the frame of reference using $\mathbf{R}$ and scale the basis functions using $\mathbf{A}$ along each direction. In essence, MAP-MRI's first basis function is a DTI tensor [4] and higher order basis functions include Hermite polynomials H_n that 'correct' the original DTI approximation. More importantly, in MAP-MRI the EAP $P(\mathbf{r})$ can be directly and analytically reconstructed once the coefficients $\mathbf{c}$ are known.

Estimation of q-space indices: Using MAP-MRI, we estimate the q-space indices as analytic integrals of the signal and EAP. We estimate the Return-To-Origin, Return-To-Axis and Return-To-Plane Probability (RTOP, RTAP and RTPP), which under several hypotheses are related to the mean pore volume, mean cross-sectional area and mean length [3].

$$RTOP \triangleq P(0) \quad (3)$$
$$RTAP \triangleq \int_{\mathbb{R}} P(R\,\mathbf{r}_{\parallel} | \mathbf{r}_{\perp} = 0) dR \quad (4)$$
$$RTPP \triangleq \int_{\mathbb{R}^2} P(R\,\mathbf{r}_{\perp} | \mathbf{r}_{\parallel} = 0) dR \quad (5)$$

We also consider quantities related to the variance of the signal and EAP: The classical Mean Squared Displacement (MSD) and the Q-space Inverse Variance (QIV) [2].

$$MSD \triangleq \int_{\mathbb{R}^3} P(\mathbf{r}) R^2 d^3\mathbf{r} = -\frac{1}{4\pi^2} \Delta E(\mathbf{q})|_{\mathbf{q}=0} \quad (6)$$
$$QIV^{-1} \triangleq \int_{\mathbb{R}^3} E(\mathbf{q}) q^2 d^3\mathbf{q} \;\; = -\frac{1}{4\pi^2} \Delta P(\mathbf{r})|_{\mathbf{r}=0} \quad (7)$$

Sensitivity Analysis: We determine the sensitivity of q-space indices by computing the partial derivative of an index value over a microstructure change, i.e., a change in axonal diameter, dispersion or volume fractions. In our experiments we perform the analysis between the following values separately: Axonal diameter $a = [1 \ldots 10]\,\mu$m, dispersion index $ODI = [0 \ldots 1]$, restricted volume fraction $\nu_{ic} = [0 \ldots 1]$ and isotropic volume fraction $\nu_{iso} = [0 \ldots 1]$. When one value is varied in our synthetic experiments, the rest is set to $a = 1\,\mu$m, $ODI = 0.05$, $\nu_{ic} = 0.9$, $\nu_{iso} = 0$. We calculate q-space and DT indices for both the multi-shell and single-shell case, where we use MAP-MRI with a radial order of 4 and 0, respectively. We repeat the experiment 200 times with a signal-to-noise ratio of 30 and average the results. We then generate the *normalized* index values by estimating all indices over a microstructure change and by dividing each by its maximum over the curve. In this way, we normalize for the magnitude differences between different indices (e.g. 10^{10} for $RTOP$ and 10^{-9} for QIV). We then calculate the derivative of the normalized index curves by fitting a spline and computing its derivative analytically.

3. EXPERIMENTS AND RESULTS

Synthetic Experiments: Figs. 1 and 2 show the normalized values and absolute derivatives of q-space and DT indices over changes in microstructure. The normalized values provide an intuition on how indices change (positively or negatively) when a particular tissue parameter is changed. We then see the amplitude of the absolute derivative as the index's sensitivity to that tissue change. The left and right columns show results on the multi-shell (MS) $b_{max} = 10,000$ s/mm^2 and single-shell (SS) $b_{max} = 1,000$ s/mm^2 data, respectively. The solid lines represent q-space indices and the dashed lines DT indices. In the axonal diameter figures (first row) we also mark the largest *in-vivo* axon diameter with a star at 4μm [10]. Diameters up to 10μm were included to be consistent with [7]. Overall, it can be seen that the normalized values for SS curves behave more monotonic than the MS curves.

Starting with axonal diameter (first row), it can be seen that their indices change little below 4μm. This corresponds to the sensitivities in Fig. 2, where the index derivative is nearly zero below 4μm. We also find that the sensitivity of RTOP and RTAP (blue and green) increases close to linearly and QIV (pink) and $D_{\perp}$ become more sensitive after 7μm. Lastly, the multi-shell q-space indices are more sensitive than the single-shell ones, and the DT indices are least sensitive.

Considering axonal dispersion (second row), we find that the multi-shell RTOP and RTAP show a small value increase at ODI lower than 0.05. This is likely caused by the nearly constant diffusion signal perpendicular to the cylinder axis with the preset volume fractions and low axonal dispersion, causing unstable MAP-MRI signal extrapolation. Then, as ODI increases, we find that MS and SS q-space indices have similar profiles, indicating that higher b-values do not clearly improve index sensitivity to dispersion. At ODI between 0.3 and 0.6 the FA (dashed brown) is the most sensitive parameter, after which all indices are similarly sensitive.

Showing changes over restricted volume fraction (third row), we find that multi-shell RTOP and RTAP are more sen-

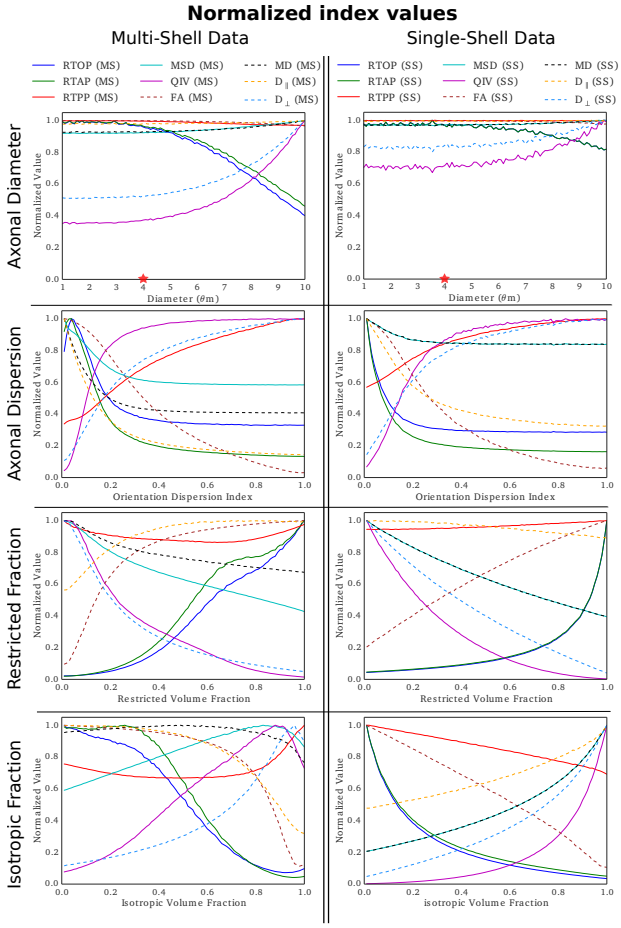

Fig. 1: Normalized q-space and DT index values over simulated microstructure change. The left and right columns show results on the multi-shell (MS) $b_{max} = 10,000\,\text{s/mm}^2$ and single-shell (SS) $b_{max} = 1,000\,\text{s/mm}^2$ data, respectively. From top to bottom we show results over axon diameter, dispersion index, and restricted and isotropic volume fractions. The stars in the axonal diameter figures indicate the largest axon diameter found *in-vivo* [10].

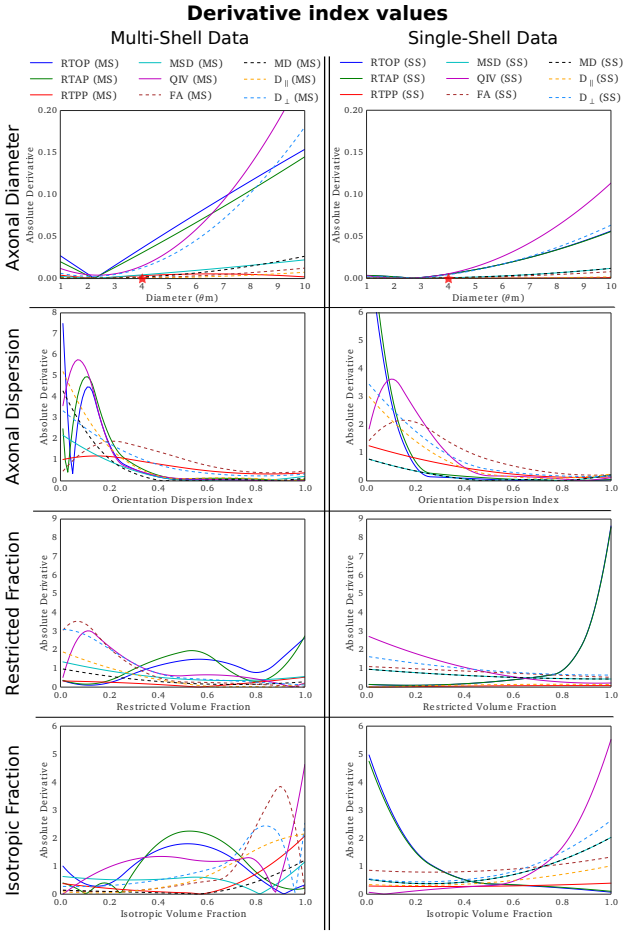

Fig. 2: The first order derivatives of q-space and DT index values over simulated microstructure change. The layout is the same as in Fig. 1.

sitivity than their single-shell versions below volume fractions of 0.8. In MS, we see that QIV (pink) and FA (dashed brown) are more sensitive at lower volume fractions while multi-shell RTOP and RTAP sensitivity dominates at volume fractions beyond 0.3. In SS RTOP and RTAP are only most sensitive beyond 0.8, while QIV dominates the curve below 0.2.

Lastly, when varying the isotropic volume fraction (fourth row) we see a similar profile as with the restricted volume fraction – only reversed. This makes sense as decreasing the restricted volume fraction and increasing the isotropic volume fraction both replace the restricted signal contribution with either an anisotropic or isotropic tensor. In MS, we see a high sensitivity for FA above 0.7, RTOP and RTAP dominate between 0.3 and 0.7, and QIV is sensitive below 0.3.

To make these results more tangible, in the next experiment we use real HCP data to show which indices are more sensitive in different areas of the brain.

HCP Experiment: We select a coronal slice of a subject of the human connectome project and use NODDI [11] to estimate the axonal dispersion and intra-axonal and isotropic volume fractions. The result can be seen in the top row of Fig. 3. For every pixel in this image we determine which q-space or DT index is most sensitive to a microstructure change *given the axonal dispersion and volume fractions found in that pixel*. The results are given separately for single-shell and multi-shell in the second and third row of Fig. 3.

To find this most sensitive index we first generate a 3-dimensional volume of synthetic dMRI voxels, varying ODI, ν_{ic} or ν_{iso} along each axis from 0 to 1, to be used as a *look-up table*. We do not include axonal diameter as we found its sensitivity is negligible (top row Fig. 2). We compute the same scalar indices as in the previous section. Then, for every voxel within the brain mask, we retrieve the partial derivatives in our synthetic volume at the position of the found NODDI

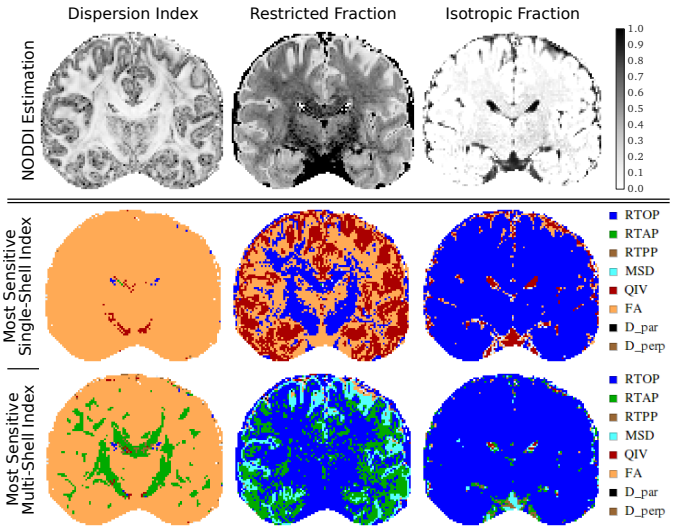

Fig. 3: A coronal slice of a subject of the HCP data. The top row shows the parameters that NODDI estimates. The bottom row shows the expected index that is most sensitive when that parameter changes.

parameters (i.e., ODI, ν_{ic} or ν_{iso}). We then find the index with the highest sensitivity and label the voxel accordingly.

The first column of Fig. 3 shows that when ODI changes, FA (brown) is most sensitive in most of the brain for both MS and SS. Only in MS is RTAP (green) more sensitive in coherent white matter (e.g. Corpus Callosum). When the restricted volume fraction is changed (second column) we find a different result between SS and MS. In SS, RTOP (blue) is most sensitive in coherent white matter, QIV (red) in the cortex and FA in the rest of the brain. In MS, RTOP is most sensitive in the bulk of the brain, and RTAP and MSD (light-blue) in the cortex. Lastly, when isotropic volume fractions change (third column) RTOP is most sensitive in most of the brain and QIV in the CSF. MD is never the most sensitive index.

4. DISCUSSION AND CONCLUSION

In this work we clarified and illustrated the sensitivity of q-space indices to changes in axonal diameter, axonal dispersion and tissue composition, for both single-shell and multi-shell acquisitions on both synthetic and real data. In Fig. 2 we showed that multi-shell q-space indices improve the sensitivity to changes in volume fraction in the range between 0.3 and 0.8, which are often found in the brain (middle column Fig. 3). Furthermore, Fig. 3 shows that RTAP is the most sensitive parameter w.r.t. dispersion in anisotropic white matter. This means that a small change in dispersion has a large effect the estimated 'apparent axon diameter' [3] – an effect which is typically ignored. Finally, and perhaps most interestingly, the single-shell results in Fig. 3 show that, when a change is expected in tissue composition, it may be more sensible to look for changes in QIV and RTOP, rather the classical FA and MD. Based on these results, it may be interesting to revisit older DT studies using QIV and RTOP as a marker for pathology.

Acknowledgments

This work was partly supported by the French ANR "MOSIFAH" under ANR-13-MONU-0009-01. Data used in the preparation of this work were obtained from the Human Connectome Project (HCP) database.

5. REFERENCES

[1] Stejskal. "Use of Spin Echoes in a Pulsed Magnetic-Field Gradient Study Anisotropic Restricted Diffusion Flow." J CHEM PHYS 43.10, pp. 3597-3603, 1965.

[2] Hosseinbor et al. "Bessel fourier orientation reconstruction (BFOR): An analytical diffusion propagator reconstruction for hybrid diffusion imaging and computation of q-space indices." NeuroImage 64 (2013): 650-670.

[3] Özarslan et al. "Mean Apparent Propagator (MAP) MRI: A novel Diffusion Imaging Method for Mapping Tissue Microstructure." NeuroImage 78, pp. 16-32, 2013.

[4] Basser et al. "Estimation of the Effective Self-Diffusion Tensor from the NMR Spin Echo." J MAGN RESON, Series B 103.3, pp. 247-254, 1994.

[5] Fick et al. "Laplacian-Regularized MAP-MRI: Improving Axonal Caliber Estimation." ISBI (2015).

[6] Ronen et al. "Microstructural organization of axons in the human corpus callosum quantified by diffusion-weighted magnetic resonance spectroscopy of N-acetylaspartate and post-mortem histology." Brain Struct Funct 219.5 (2014): 1773-1785.

[7] Drobnjak et al. "PGSE, OGSE, and sensitivity to axon diameter in diffusion MRI: Insight from a simulation study." MRM (2015).

[8] Setsompop et al. "Pushing the limits of in vivo diffusion MRI for the Human Connectome Project." NeuroImage 80, pp. 220-233, 2013.

[9] Zhang et al. "Axon diameter mapping in the presence of orientation dispersion with diffusion MRI." Neuroimage 56.3 (2011): 1301-1315.

[10] Aboitiz et al. "Fiber composition of the human corpus callosum." Brain research 598.1, pp. 143-153, 1992.

[11] Zhang et al. "NODDI: practical in vivo neurite orientation dispersion and density imaging of the human brain." Neuroimage 61.4 (2012): 1000-1016.